A MATLAB®-based Object-Oriented Approach to Multipath Fading Channel Simulation

Cyril-Daniel Iskander*
Hi-Tek Multisystems
7945 Avenue de Cornouailles, Québec, QC, Canada, G1H 3V9
E-mail: cyril_iskander@hotmail.com

Abstract— **A MATLAB®-based object-oriented implementation of a multipath fading simulator is presented. The simulator uses the interpolated filtered Gaussian noise approach to emulate the time selectivity of the channel (i.e. the Doppler spreading), and a bandlimited representation of the channel to efficiently emulate the frequency selectivity of the channel (i.e. the time spreading).**

I. Introduction

Multipath fading channel simulators are essential components of wireless systems physical layer simulations. This paper presents a MATLAB®-based approach to multipath fading channel simulation.

The next section presents an overview of popular methodologies for the simulation of multipath fading channels. Two effects must be simulated: the time selectivity of the channel (Doppler spreading) due to motion, and the frequency selectivity (time spreading) due to resolvable multipath components. Simulation approaches are reviewed for both these tasks.

The third section presents an overview of the simulation methodology used in our particular channel simulator. In particular, the simulator employs an interpolated filtered Gaussian noise source to simulate the Doppler spreading, followed by a bandlimited channel transformation to efficiently simulate the multipath dispersion. Both Rayleigh and Rician processes can be generated, for a set of different Doppler spectra. Speed/accuracy tradeoffs and optimizations specific to this simulator are discussed, such as the combination of linear and polyphase interpolation filtering, and the truncation of the bandlimited filter.

Section IV presents the application programming interface, along with channel object properties. Examples illustrate how to create channel objects, use them in a simulation, and visualize simulation quantities using the channel visualization tool.

Simulation examples are given in Section V. The statistical performance is evaluated in terms of the simulated fading processes' probability distributions, Doppler spectra and autocovariances.

II. Review of Multipath Fading Channel Simulation Techniques

A. Physical Modeling of Multipath Fading Channels

The most common model used in the radio communications literature to describe flat fading in urban/suburban environments is Clarke's model [1]. It assumes a fixed transmitter with a vertically polarized antenna, and a mobile terminal. The electric field incident on the mobile antenna consists of N azimuthal plane waves (also often called *scatterers*), with:

- Arbitrary carrier phases ϕ_n;
- Arbitrary azimuthal angles of arrivals α_n;
- Equal average amplitudes.

Mathematically, this field can be expressed as:

$$\begin{aligned} E_z(t) &= \sum_{n=1}^{N} E_n(t) = \sum_{n=1}^{N} \bar{E}_n C_n \cos(2\pi f_c t + \theta_n) \\ &= T_c(t)\cos(2\pi f_c t) - T_s(t)\sin(2\pi f_c t) \end{aligned} \quad (1)$$

where $T_c(t) = \bar{E}\sum_{n=1}^{N} C_n \cos(\theta_n)$ and $T_s(t) = \bar{E}\sum_{n=1}^{N} C_n \sin(\theta_n)$ are the uncorrelated in-phase and quadrature components of the electric field, respectively, $\bar{E}_n = \bar{E}$, $n = 0, 1, \ldots, N$, are assumed to be constant, and C_n are mutually independent normalized random variables representing the fading on each path, such that $E[\sum_{n=1}^{N} C_n^2] = 1$, where $E[\cdot]$ denotes statistical expectation. $\theta_n = 2\pi f_n t + \phi_n$ are the phases, with $f_n = (v/\lambda)\cos\alpha_n$ the Doppler shift of the n^{th} wave, given a mobile speed v (m/s), a carrier frequency f_c (Hz) and a carrier wavelength $\lambda = c/f_c$ ($c \simeq 3.10^8$ m/s is the speed of light in free space). $f_d = v/\lambda$ is called the maximum Doppler shift. For a large number of waves N, as per the central limit theorem ([2], p. 266), samples T_c and T_s of the in-phase and quadrature processes $T_c(t)$ and $T_s(t)$ become normally distributed with zero means and variances $E[T_c^2] = E[T_s^2] = \bar{E}^2/2 = \Omega/2 = \sigma^2$. Hence the envelope of a sample E_z of the electric field $E_z(t)$:

$$r = |E_z| = \sqrt{T_c^2 + T_s^2} \quad (2)$$

where $|\cdot|$ denotes the absolute value of $\cdot$, can be shown ([2], p. 195) to be Rayleigh-distributed, i.e. with probability density function (pdf):

$$p_R(r) = \frac{2r}{\Omega} e^{-\frac{r^2}{\Omega}}, \quad r \geq 0 \quad (3)$$

and cumulative distribution function (cdf):

$$F_R(r) = 1 - e^{-\frac{r^2}{\Omega}} \quad (4)$$

where $\Omega = 2\sigma^2 = E[r^2]$. The quantity $\tan^{-1}(T_s/T_c)$ can be shown ([2], pp. 200-201) to be independent of r and uniformly distributed over $[-\pi/2, \pi/2]$. By periodicity, the phase

*Formerly with The MathWorks, Natick, MA.

of E_z, θ, is then independent of r and uniformly distributed over $[0, 2\pi]$:

$$p_\Theta(\theta) \quad = \quad \frac{1}{2\pi}, \quad 0 \le \theta \le 2\pi. \tag{5}$$

If a dominant stationary wave $E_0(t) = \bar{E}_0 C_0 \cos(2\pi f_c t + \theta_0)$ of constant amplitude $A = \bar{E}_0 C_0$ is included in the received signal (e.g. a nonfading line-of-sight component), the expression for the electric field becomes:

$$E_z(t) \quad = \quad E_0(t) + \sum_{n=1}^{N} \bar{E}_n C_n \cos(2\pi f_c t + \theta_n) \tag{6}$$

The envelope r can then be shown ([2], pp. 196-197) to be Rician-distributed, i.e. with pdf:

$$p_R(r) \quad = \quad \frac{2r}{\Omega} e^{-\frac{A^2+r^2}{\Omega}} I_0\left(\frac{2Ar}{\Omega}\right), \quad r \ge 0 \tag{7}$$

and cdf:

$$F_R(r) \quad = \quad 1 - Q_1\left(\frac{A}{\sqrt{\Omega/2}}, \frac{r}{\sqrt{\Omega/2}}\right) \tag{8}$$

where $I_0(\cdot)$ is the modified Bessel function of order 0, and $Q_1(\cdot)$ is the Marcum-Q function of order 1. $K_r = A^2/\Omega$ is termed the *Rician K-factor*. When $A = 0$ (i.e. $K_r = 0$), the Rice pdf reverts to the Rayleigh pdf. Note that the Rice pdf was also independently discovered by Nakagami [3] in his studies of mobile radio propagation, which he termed the n-distribution. Hence the Rice pdf is also called the Nakagami-n or Nakagami-Rice pdf. The pdf of the phase of E_z can be shown ([2], pp. 499-501) to be given by ($\phi_0 = 0$):

$$\begin{aligned} p_\Theta(\theta) \quad = \quad & \frac{e^{-\frac{A^2}{2\sigma^2}}}{2\pi} + \frac{A\cos(\theta) e^{-\frac{A^2 \sin^2(\theta)}{2\sigma^2}}}{2\sigma\sqrt{2\pi}} \\ & \times \left[1 + 2\text{erf}\left(\frac{A\cos(\theta)}{\sigma}\right)\right], \quad 0 \le \theta \le 2\pi \end{aligned} \tag{9}$$

where $\text{erf}(x) = 2/\sqrt{\pi} \int_0^x e^{-z^2} dz$ is the error function.

Based on Clarke's model, Gans [4] developed a power spectral theory for the mobile radio channel. Assuming that N is very large, that the α_n's are uniformly distributed over $[0, 2\pi]$, and that the signal is transmitted by an omnidirectional vertical $\lambda/4$ antenna with gain $G(\alpha) = 1.5$, the power spectral density (PSD) of the electric field Eq. (1) was shown to be (c.f. [5], Eq. 1.2-11):

$$S(f) \quad = \quad \frac{1.5\Omega}{2\pi f_d \sqrt{1 - (\frac{f - f_c}{f_d})^2}}. \tag{10}$$

The PSD of the electric field for the Rician case is similar to that of the Rayleigh case, but with an impulse at frequency f_c.

In the model developed above, it is assumed that the scatterers are not resolved by the receiver, hence from the receiver's perspective the channel has only one propagation path, and it is said to exhibit frequency-flat fading. If groups of scatterers are resolvable at the receiver, then the channel has multiple propagation paths, and it is said to exhibit frequency-selective fading. A frequency-flat fading channel simulator needs to reproduce only the Doppler spreading, while a frequency-selective fading channel simulator needs to emulate both Doppler spreading and time spreading. In the general case, the Doppler spreading and time spreading are mutually related. However, for simplicity most channel simulators treat the two spreading processes independently. Such simulators are said to follow the Wide-Sense Stationary Uncorrelated Scattering (WSSUS) assumption put forth in [6]. In the sections below, common approaches are reviewed for separately simulating the Doppler spreading process and the time spreading process.

B. Doppler Spreading Simulation

The simulated stochastic fading process given by Eq. (1) needs to have (at least) the following properties:

- Since it is a complex Gaussian process, its envelope should be Rayleigh-distributed.
- Due to the Doppler spreading, its power spectrum is given by Eq. (10) for the Clarke model, or by any other specified spectrum (c.f. some examples in Section III-C.2).

Among the Rayleigh and Rician fading simulators designed to ensure that the above two properties are approximately verified, most fall within one of the two following categories: sum-of-sinusoids (SoS) simulators and filtered Gaussian noise (FGN) simulators.

B.1 Sum-of-Sinusoids Simulators

Many sum-of-sinusoids methods have been proposed for fading channel simulation over the past three decades. The rationale is to create a fading process by superposing several waves, each one being characterized by an amplitude, an angle of arrival, and a phase (as in Clarke's physical model). By the central limit theorem, the resulting process will tend towards a Gaussian distribution. Hereby we briefly review some of the more popular methods.

Deterministic Simulation Models

A deterministic simulation model is one in which all parameters of the simulation (amplitudes, angles of arrivals, and phases) are deterministic quantities: hence the same fading waveform is reproduced for every trial run of a simulation. The classic Jakes fading simulator [5] is an example of an early deterministic SoS simulator. However, it is by now well known that it leads to in-phase and quadrature components of the complex fading process which are correlated, which is not desirable. The modified Jakes simulator of [7] suffers from the same problem. However, the SoS simulator of [8], recognizing the deficiencies of previous Jakes-type simulators, produces uncorrelated in-phase and quadrature components.

Stochastic Simulation Models

A stochastic simulation model is one in which at least one parameter is a random quantity. In most stochastic simulation

models, at the beginning of a simulation trial, one or more parameters are generated randomly, but they are then held fixed throughout the rest of the simulation trial: hence the simulator can be viewed as deterministic conditional on the initial set of random parameters.

The motivation for using SoS simulators comes from Rice's method [9], [10], which allows a Gaussian process $\mu_i(t)$ to be generated according to (using the notation of [11]):

$$\mu_i(t) \quad = \quad \lim_{N_i \to \infty} \sum_{n=1}^{N_i} c_{i,n} \cos(2\pi f_{i,n} t + \theta_{i,n}), \quad (11)$$

where the gains $c_{i,n} = 2\sqrt{\Delta f_i S_{\mu\mu}(f_{i,n})}$ and the frequencies $f_{i,n} = n\Delta f_i$ are fixed quantities, while the phases $\theta_{i,n}$ are uniformly distributed random variables. The frequency interval Δf_i is chosen such that $N_i \Delta f_i$ covers the frequency range occupied by the PSD $S_{\mu\mu}(f)$ of $\mu_i(t)$. A complex Gaussian process can then be obtained as $\mu(t) = \mu_1(t) + j\mu_2(t)$.

A practical simulator uses only a finite number of sinusoids, hence

$$\mu_i(t) \quad = \quad \sum_{n=1}^{N_i} c_{i,n} \cos(2\pi f_{i,n} t + \theta_{i,n}). \quad (12)$$

It is shown in [12] that only when the gains $c_{i,n}$ and the frequencies $f_{i,n}$ are constant, and the phases $\theta_{i,n}$ are random variables, is the resulting process stationary, mean-ergodic, and autocorrelation-ergodic.

B.2 Filtered Gaussian Noise Simulators

A complex Gaussian fading process with desired spectral properties can be "directly" simulated by generating a complex Gaussian process and filtering it with a Doppler filter.

The Doppler filter should be designed to produce (approximately) the desired Doppler spectrum. Both finite impulse response (FIR) filters and infinite impulse response (IIR) filters have been proposed for the simulation of Doppler spreading. FIR filters are not subject to stability problems, but require many coefficients to closely approximate the desired spectrum [13], [14]. Also, closed-form expressions for the Doppler filter can be found in certain cases. IIR filters require less coefficients, but can lead to instability, although methods have been proposed to mitigate the risk of instability [15], [16], [17], [18], [19].

The filtering operation can be carried out in the time domain or the frequency domain. Time-domain simulators include [13] and [14], and perform (in the case of FIR filters) direct linear convolution of the generated complex Gaussian process with the impulse response of the Doppler filter. Frequency-domain simulators use the Fast Fourier Transform (FFT) to perform convolution [20], [21], [22]. This speeds up simulation for large blocks of samples to be generated, but inherently requires that samples be produced as blocks, which can introduce larger delays and consume more memory.

C. Time Spreading Simulation

One approach to time spreading simulation consists in constructing a channel filtering impulse response with a spacing between points which is the smallest common denominator of [11]:

- The smallest resolvable delay in the channel impulse response.
- The input signal sample size.

As explained in Section III-A, this can be inefficient.

Another approach [14], [23] consists in transforming the channel impulse response into an equivalent symbol-spaced impulse response, as reviewed in Section III-B. This can reduce the length of the impulse response, as compared to the previous approach.

D. Comparison

In this section we briefly compare the SoS and FGN methods, in terms of accuracy, delay, and speed:

- For the SoS method, certain Doppler spectra such as the Jakes and Gaussian spectra can be reproduced with good accuracy [11]. However, apart from Rice's method (in which the number of sinusoids tends to infinity), there is no well-known method for obtaining arbitrary Doppler spectra, for a stationary, mean- and autocorrelation-ergodic simulator (the Monte-Carlo method of [24] is non-autocorrelation-ergodic [12]). In contrast, the FGN method allows for arbitrary Doppler spectra to be specificied, as long as the Doppler filter impulse response has enough coefficients: for very small fading rates, long impulse responses may be needed.
- The SoS method generates the fading process sample-by-sample, hence there is no significant delay in the simulation. The FGN method does require a block of input samples to be available (especially if frequency-domain filtering is used), hence some delay is introduced: however the size of the block of samples can be adjusted.
- To obtain a satisfactory accuracy, several tens (or hundreds) of sinusoids usually need to be generated in the SoS method, which is computationally cumbersome (although some "fast" SoS simulators based on a table-lookup approach can be devised [11]). The FGN approach only requires filtering to be performed, for which many computational efficient approaches exist.

In our implementation, we chose the FGN approach, hence allowing more flexibility in the specification of the Doppler spectra.

III. Simulation Methodology

A. Discrete Multipath Channel Model

A discrete multipath channel simulator is appropriate to emulate a set of discrete resolvable multipath components (scattering and reflections from smaller structures) [14]. A popular model for a discrete multipath channel is the tapped-delay-line (TDL) channel model [25], [26]. In the TDL model, the low-pass impulse response of the channel is modeled as:

$$\tilde{c}(\tau(t), t) \quad = \quad \sum_{k=1}^{K(t)} \tilde{a}_k(\tau_k(t), t) \delta(\tau - \tau_k(t)), \quad (13)$$

where $K(t)$ is the time-varying number of multipaths, $\tilde{a}_k(\tau_k(t), t) = a_k(t) e^{-j2\pi f_c \tau_k(t)}$ are the low-pass time-varying

complex channel coefficients (including both amplitude and phase effects), $\tau_k(t)$ are the time-varying delays, f_c is the carrier frequency. If the delays and number of discrete components are assumed to be time-invariant, i.e. $K(t) = K$ and $\tau_k(t) = \tau_k$, then the impulse response simplifies to:

$$\tilde{c}(\tau, t) \quad = \quad \sum_{k=1}^{K} \tilde{a}_k(t)\delta(\tau - \tau_k). \tag{14}$$

If $\tilde{s}(t)$ is a lowpass input to a TDL channel, then the lowpass output $\tilde{y}(t)$ is obtained as the convolution between $\tilde{s}(t)$ and $\tilde{c}(\tau, t)$:

$$\tilde{y}(t) = \tilde{s}(t) * \tilde{c}(\tau, t) = \sum_{k=1}^{K} \tilde{a}_k(t)\tilde{s}(\tau - \tau_k). \tag{15}$$

A TDL channel model is illustrated in Fig. 1 [14].

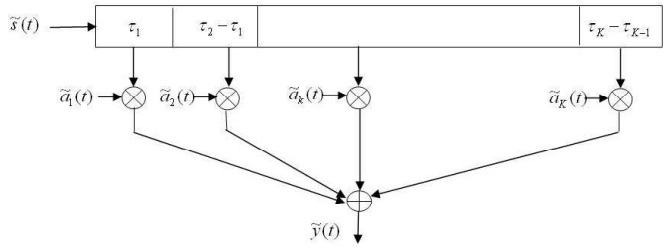

Fig. 1. Tapped-delay-line channel model with variable tap spacings.

The following situations can arise in a practical simulation scenario:

- The delays τ_k are not integer multiples of the simulation sampling time T_s, or some of the differential delays $\tau_k - \tau_i$ may be equal to a small fraction of the simulation sampling time T_s.
- The number of paths is very large.

In the first case, one needs to generate samples at a possibly much higher rate than the simulation sampling rate $1/T_s$, which is inefficient. In the second case, the high number of paths also puts a burden on the computational complexity of the simulator. The next section details a method which trades off accuracy for simulation speed, by employing a bandlimited discrete multipath channel model.

B. Time Spreading Simulation: Bandlimited Discrete Multipath Channel Model

A more efficient way of modeling a frequency-selective fading channel with variable delays is by using an equivalent uniformly spaced tapped delay line. To do so, assume that the lowpass input $\tilde{s}(t)$ to the channel (i.e. the transmitted signal) is bandlimited to a bandpass (2-sided) bandwidth B. Then $\tilde{s}(t)$ can be expressed in terms of its samples as (using a sampling rate of $B = 1/T_s = R_s$ samples per second):

$$\tilde{s}(t - \tau) = \sum_{n=-\infty}^{\infty} \tilde{s}(t - nT_s)\text{sinc}(B(\tau - nT_s)). \tag{16}$$

Then the lowpass signal at the channel output is:

$$\begin{aligned}
\tilde{y}(t) &= \int_{-\infty}^{\infty} \tilde{c}(\tau, t)\tilde{s}(t - \tau)d\tau \\
&= \int_{-\infty}^{\infty} \tilde{c}(\tau, t) \sum_{n=-\infty}^{\infty} \tilde{s}(t - nT_s)\text{sinc}(B(\tau - nT_s))d\tau \\
&= \sum_{n=-\infty}^{\infty} \tilde{s}(t - nT_s) \int_{-\infty}^{\infty} \tilde{c}(\tau, t)\text{sinc}(B(\tau - nT_s))d\tau \\
&= \sum_{n=-\infty}^{\infty} \tilde{s}(t - nT_s)\tilde{g}_n(t)
\end{aligned} \tag{17}$$

where:

$$\begin{aligned}
\tilde{g}_n(t) &= \int_{-\infty}^{\infty} \tilde{c}(\tau, t)\text{sinc}(B(\tau - nT_s))d\tau \\
&= \int_{-\infty}^{\infty} \left(\sum_{k=1}^{K} \tilde{a}_k(t)\delta(\tau - \tau_k) \right) \text{sinc}(B(\tau - nT_s))d\tau \\
&= \sum_{k=1}^{K} \tilde{a}_k(t)\text{sinc}(B(\tau_k - nT_s)) \\
&= \sum_{k=1}^{K} \tilde{a}_k(t)\alpha(k, n)
\end{aligned} \tag{18}$$

with:

$$\alpha(k, n) = \text{sinc}(B(\tau_k - nT_s)) = \text{sinc}(\tau_k/T_s - n), \tag{19}$$

for $k = 1, 2, \ldots, K$. Hence, the variable-delay TDL channel is transformed into an equivalent uniform-delay TDL channel, where inputs are sampled at $T_s = 1/B$ and multiplied by the tap-gain processes $\tilde{g}_n(t)$.

For practical purposes, the convolution sum to compute $\tilde{y}(t)$ must be truncated to a finite number of terms. It is seen that the coefficients $\{\alpha(k, n)\}$ decrease rapidly (since the sinc function decreases rapidly). Hence one approach to truncation is to set a threshold such that tap-gain processes having a set of coefficients $\{\alpha(k, n)\}$ less than that threshold are discarded. Then the equation governing the bandlimited discrete multipath channel model becomes:

$$\tilde{y}(t) \quad = \quad \sum_{n=-N_1}^{N_2} \tilde{s}(t - nT_s)\tilde{g}_n(t) \tag{20}$$

where now $\tilde{g}_n(t) = \tilde{a}_k(t)\alpha(k, n)$, $-N_1 \leq n \leq N_2$, and $\alpha(k, n) = \text{sinc}(\tau_k/T_s - n)$, $k = 1, 2, \ldots, K$, $-N_1 \leq n \leq N_2$. A bandlimited TDL channel model is illustrated in Fig. 2 [14].

The discrete-time implementation of (20), with a sampling period of $T_s = 1/R_s$, can be expressed as:

$$\tilde{y}[i] \quad = \quad \sum_{n=-N_1}^{N_2} \tilde{s}[i - n]\tilde{g}_n[i], \tag{21}$$

where $\tilde{s}[i] = \tilde{s}(iT_s)$ and $\tilde{g}_n[i] = \tilde{g}(iT_s)$, $i = 0, 1, 2, \ldots$.

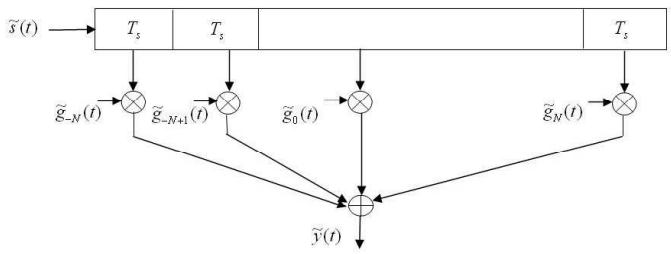

Fig. 2. Bandlimited tapped-delay-line channel model with equal spacings.

For a block of N samples, the equation above can be put in matrix form as:

$$\tilde{\mathbf{y}} \quad = \quad \sum_{columns} \tilde{\mathbf{g}} . * \mathbf{U} \tag{22}$$

where $.*$ denotes element-wise matrix multiplication, and

$$\tilde{\mathbf{g}} = \alpha \times \tilde{\mathbf{a}} \tag{23}$$

where:

$$\alpha = \begin{bmatrix} \alpha(1,-N_1) & \alpha(2,-N_1) & \dots & \alpha(K,-N_1) \\ \alpha(1,-N_1+1) & \alpha(2,-N_1+1) & \dots & \alpha(K,-N_1+1) \\ \vdots & \vdots & \ddots & \vdots \\ \alpha(1,N_2) & \alpha(2,N_2) & \dots & \alpha(K,N_2) \end{bmatrix}$$

and

$$\tilde{\mathbf{a}} = \begin{bmatrix} \tilde{a}_1(1) & \tilde{a}_1(2) & \dots & \tilde{a}_1(N) \\ \tilde{a}_2(1) & \tilde{a}_2(2) & \dots & \tilde{a}_2(N) \\ \vdots & \vdots & \ddots & \vdots \\ \tilde{a}_K(1) & \tilde{a}_K(2) & \dots & \tilde{a}_K(N) \end{bmatrix}.$$

Also:

$$\mathbf{U} \quad = \quad \begin{bmatrix} \tilde{s}(1) & \tilde{s}(2) & \dots & \tilde{s}(N) \\ u(1) & \tilde{s}(1) & \dots & \tilde{s}(N+1) \\ u(2) & u(1) & \dots & \tilde{s}(N+2) \\ \vdots & \vdots & \ddots & \vdots \\ u(N_1+N_2) & \dots & \dots & \tilde{s}(N-(N_1+N_2)) \end{bmatrix}$$

where $\mathbf{u} = [u(1)u(2)\dots u(N_1+N_2)]^T$ is the input state vector at the beginning of the block. Eq. (22) can be calculated in MATLAB® as:

```
y = sum(g.*U, 1)
```

It is seen that the tap-gain processes $\{\tilde{g}_n(t)\}$ depend on the sampling rate $B = 1/T_s = R_s$. It is thus necessary to understand how the latter must be chosen. Let T denote the input symbol period and $R = 1/T$ the input symbol rate. Let the input signal be input to a transmitter filter, which is assumed to be a raised-cosine (RC) - or root-raised cosine (RRC) - filter with excess factor β. Then the (two-sided) bandwidth of the input signal after pulse filtering is given by $B_r = \frac{1+\beta}{T}$. According to Nyquist's sampling theorem, we must have $R_s > 2\frac{B_r}{2} = \frac{1+\beta}{T}$. If $\beta = 0$, which corresponds to sinc pulse shaping, then the minimum sampling rate is $R_{s,min} = 1/T = R$. Then for each input symbol, only one sample is needed by the bandlimited channel model. If $\beta = 1$, which corresponds to the highest excess factor for a raised-cosine filter, then the minimum sampling rate is $R_{s,min} = 2/T = 2R$. Then for each input symbol, two samples must be taken and input to the bandlimited channel model. Hence to accommodate all excess factors for the special but important case of an RC (or RRC) filter, oversampling by a factor of two must occur at the transmitter side, in order for the bandlimited channel model to be accurate.

The generation of the fading processes $\tilde{a}_k(t)$, $k = 1, 2, \dots, K$, is detailed in the next section.

C. Doppler Spreading Simulation: Interpolated Filtered Gaussian Noise Model

For a Rayleigh fading channel, each fading process $\tilde{a}_k(t)$ is complex Gaussian, with a Doppler power spectrum $S_k(f)$. While different $\tilde{a}_k(t)$'s can have distinct Doppler power spectra, such as in the COST 207 channel models [27], for clarity we assume in the following that all paths have the same Doppler spectrum, i.e. $S_k(f) = S(f)$, $k = 1, 2, \dots, K$.

A methodology to simulate a Rayleigh fading channel consists in shaping a complex Gaussian noise source by the appropriate Doppler power spectrum. The resulting process is then interpolated to the input signal sampling rate. The interpolated filtered Gaussian noise (IFGN) approach can be summarized as follows, for each fading process:

- Generate a complex Gaussian process with variance 1 (the real and imaginary part each have variance 1/2).
- Filter the process with a Doppler filter with frequency response $H(f) = \sqrt{S(f)}$ and impulse response $h(t) = F^{-1}(H(f))$, where $F^{-1}(\cdot)$ denotes inverse Fourier transform. The impulse response is sampled at a rate f_s, to obtain a discrete-time impulse response $\{h[n]\}$.
- Interpolate the discrete-time FGN process of rate $f_s = 1/t_s$ to match the input signal sampling rate R_s, using a combination of polyphase and linear interpolation filtering.
- Scale the interpolated FGN sequence to obtain the desired average power gain for the given path.

The complex Gaussian noise generation, Doppler filtering, interpolation filtering, and path gain scaling steps are detailed below.

C.1 Complex Gaussian Noise Generation

Let $x_{G,R}(t)$ and $x_{G,I}(t)$ denote two real uncorrelated Gaussian processes with zero-mean and common variance 1/2. Their discrete-time versions $x_{G,R}[n] = x_{G,R}(t = nt_s)$ and $x_{G,I}[n] = x_{G,I}(t = nt_s)$ are generated using a pseudorandom Gaussian random number generator, such as Marsaglia's Ziggurat algorithm [28]. A complex Gaussian noise process with variance 1 is then obtained as $x_G[n] = x_{G,R}[n] + jx_{G,I}[n]$.

C.2 Doppler Filtering

The purpose of the Doppler filter is to shape the generated complex Gaussian noise process such that the filtered process has the desired Doppler power spectrum. Several common power spectra models for fading processes are reviewed below, along with their theoretical/empirical motivation and areas of application. Theoretical expressions are given for the power spectral density (PSD) and autocorrelation function (ACF) of the fading processes.

Jakes Doppler Spectrum

The so-called "Jakes" Doppler power spectrum model is actually due to Gans [4], which analyzed Clarke's model [1] for a mobile fading channel. Interestingly, it is in turn explained in [29] how Clarke's model draws from earlier work by Gilbert [30], and it is advocated in [29] to rename the classical mobile fading channel model as "Gilbert's model". The Clarke-Gilbert model is also called the "classical model". The Jakes Doppler spectrum applies to a mobile receiver. It follows from the following assumptions [11]:

- The radio waves propagate horizontally.
- At the receiver, the angles of arrival of the radio waves are uniformly distributed over $[-\pi, \pi]$.
- At the receiver, the antenna is omnidirectional, i.e. the antenna pattern is circular-symmetrical.

The baseband normalized Jakes Doppler spectrum is given analytically by:

$$S_j(f) = \frac{1}{\pi f_d \sqrt{1-(f/f_d)^2}}, \ |f| \leq f_d \tag{24}$$

where f_d is the maximum Doppler shift. The corresponding autocorrelation is:

$$R_j(\tau) = J_0(2\pi f_d \tau) \tag{25}$$

where $J_0(z)$ is the Bessel function of the first kind of order 0 ([31], Eq. 3.715.19). The amplitude of the frequency response is then given by $|H_j(f)| = \sqrt{S_j(f)}$, and the impulse response can be derived as ([31], Eq. 3.715.19):

$$h_j(t) = \Gamma(3/4)\left(\frac{f_d}{\pi|t|}\right)^{1/4} J_{1/4}(2\pi f_d|t|) \tag{26}$$

where $\Gamma(\cdot)$ is the gamma function. The value of $h_j(t)$ at $t=0$ is calculated as $\lim_{t\to\infty} h_j(t) = \Gamma(3/4)/\Gamma(5/4) f_d^{1/2}$. The discrete-time impulse response used for simulation is a sampled, truncated (to M points), causal (delayed by $M/2$ points) version of $h_j(t)$, given by:

$$\begin{aligned} h_j[m] &= h_j(t=(m-M/2)t_s), \\ &= \Gamma(3/4)\left(\frac{f_d}{\pi|(m-M/2)t_s|}\right)^{1/4} \\ &\quad \times J_{1/4}(2\pi f_d|(m-M/2)t_s|), \end{aligned} \tag{27}$$

for $m = 0, 1, \ldots, M-1$.

Flat Doppler Spectrum

It was shown in [32] that in a 3-D isotropic scattering environment, i.e. where the angles of arrival are uniformly distributed in the elevation plane and the azimuth plane (the joint pdf of the elevation angle θ and the azimuthal angle α is $p_{\theta,\alpha}(\theta,\alpha) = \frac{\sin(\theta)}{4\pi}$, $0 \leq \theta < \pi$, $0 \leq \alpha < 2\pi$, the Doppler spectrum is found theoretically to be flat. A flat Doppler spectrum is also specified in some cases of the ANSI J-STD-008 reference channel models for PCS applications, for both outdoor (pedestrian) and indoor (commercial) [33]. The baseband normalized flat Doppler spectrum is given by:

$$S_f(f) = \frac{1}{2f_d}, \ |f| \leq f_d, \tag{28}$$

and its autocorrelation by:

$$R_f(\tau) = \text{sinc}(2f_d\tau). \tag{29}$$

The impulse response of the flat Doppler filter can be derived as:

$$h_f(t) = \sqrt{2f_d}\text{sinc}(2f_d t). \tag{30}$$

The corresponding discrete-time impulse response used for simulation is:

$$h_f[m] = \sqrt{2f_d}\text{sinc}(2f_d(m-M/2)t_s), \tag{31}$$

for $m = 0, 1, \ldots, M-1$.

Gaussian Doppler Spectrum

The Gaussian power spectrum has been observed to be a good model for multipath components with long delays in UHF communications [34]. It has also been proposed for the HF channel [35], [36], [37] and the aeronautical channel at VHF-band [38], [39]. A Gaussian Doppler spectrum is also specified in some cases of the ANSI J-STD-008 reference channel models for PCS applications, for both outdoor (wireless loop) and indoor (residential, office) [33]. The baseband normalized Gaussian Doppler spectrum is given by:

$$S_g(f) = \frac{1}{\sqrt{2\pi\sigma_g^2}} \exp\left(-\frac{f^2}{2\sigma_g^2}\right), \tag{32}$$

or by the alternate representation:

$$S_g(f) = \frac{1}{f_c}\frac{\ln(2)}{\pi} \exp\left(-(\ln(2))\left(\frac{f}{f_c}\right)^2\right), \tag{33}$$

where $f_c = \sigma_g\sqrt{2\ln(2)}$ is the 3-dB cutoff frequency. The corresponding autocorrelation is:

$$R_g(\tau) = \exp(-2\pi^2\sigma_g^2\tau^2). \tag{34}$$

The Gaussian Doppler filter impulse response can be derived as:

$$h_g(t) = (2\pi)^{1/4}\sqrt{\sigma_g}\exp(-4\pi^2\sigma_g^2 t^2). \tag{35}$$

The corresponding discrete-time impulse response used for simulation is:

$$h_g[m] = (2\pi)^{1/4}\sqrt{\sigma_g}\exp(-4\pi^2\sigma_g^2((m-M/2)t_s)^2), \quad (36)$$

for $m = 0, 1, \ldots, M-1$.

Symmetrical Restricted Jakes Doppler Spectrum

The Jakes Doppler spectrum is based on the assumption that the angles of arrival at the mobile receiver are uniformly distributed [1], where the spectrum covers the frequency range from $-f_d$ to f_d. When the angles of arrival are not uniformly distributed, the Jakes Doppler spectrum does not cover the full Doppler bandwidth from $-f_d$ to f_d [29]. This also corresponds to the case of a directional antenna pattern. We denote this type of spectrum as restricted Jakes [11]. We consider here the case of symmetrical Doppler spectrum, which leads to a real impulse response. The baseband normalized restricted Jakes Doppler spectrum is given analytically by:

$$\begin{aligned} S_{rj}(f) &= \frac{A_{rj}}{\pi f_d\sqrt{1-(f/f_d)^2}}, \\ & 0 \le f_{d,min} \le |f| \le f_{d,max} \le f_d \end{aligned} \quad (37)$$

with:

$$A_{rj} = \frac{\pi/2}{\sin^{-1}\left(\frac{f_{d,max}}{f_d}\right) - \sin^{-1}\left(\frac{f_{d,min}}{f_d}\right)} \quad (38)$$

being a normalization factor. $f_{d,min}$ and $f_{d,max}$ denote the minimum and maximum positive frequencies where the spectrum is non-zero (with $-f_{d,min}$ and $-f_{d,max}$ being the corresponding negative frequencies). These frequencies can be determined from the pdf of the angles of arrival [29]. The autocorrelation can be obtained as:

$$R_{rj}(\tau) = A_{rj}\frac{2}{\pi}\int_{\sin^{-1}\left(\frac{f_{d,min}}{f_d}\right)}^{\sin^{-1}\left(\frac{f_{d,max}}{f_d}\right)} \cos(2\pi f_d\tau\sin\phi)d\phi. \quad (39)$$

The amplitude of the frequency response is given by $|H_{rj}(f)| = \sqrt{S_{rj}(f)}$, i.e.:

$$\begin{aligned} |H_{rj}(f)| &= \left[\frac{A_{rj}}{\pi f_d\sqrt{1-(f/f_d)^2}}\right]^{1/2}, \\ & 0 \le f_{d,min} \le |f| \le f_{d,max} \le f_d. \end{aligned} \quad (40)$$

A closed-form expression for the impulse response $h_{rj}(t)$ cannot be found. Hence its sampled version $h_{rj}[m] = h_{rj}(t = (m-M/2)t_s)$ is evaluated numerically by performing an inverse FFT on the frequency-sampled version of $|H_{rj}(f)|$.

Asymmetrical Jakes Doppler Spectrum

The section above on restricted Jakes Doppler spectrum modeling assumed the spectrum to be symmetrical. Examples of asymmetrical Jakes Doppler spectra can be found in [4] for the case of directional ("beam") antennas, in [40], [41] for the case of aeronautical radio channels, or in [11] for the case of satellite mobile radio channels. We consider here the case of an asymmetrical Jakes Doppler spectrum, which leads to a complex impulse response. We define the baseband normalized asymmetrical Jakes Doppler spectrum as:

$$\begin{aligned} S_{aj}(f) &= \frac{A_{aj}}{\pi f_d\sqrt{1-(f/f_d)^2}}, \\ & -f_d \le f_{d,min} \le f \le f_{d,max} \le f_d \end{aligned} \quad (41)$$

with:

$$A_{aj} = \frac{\pi}{\sin^{-1}\left(\frac{f_{d,max}}{f_d}\right) - \sin^{-1}\left(\frac{f_{d,min}}{f_d}\right)} \quad (42)$$

being a normalization factor. $f_{d,min}$ and $f_{d,max}$ denote the minimum and maximum frequencies where the spectrum is non-zero. The autocorrelation can be obtained as:

$$\begin{aligned} R_{aj}(\tau) &= \frac{A_{aj}}{\pi}\left[\int_{\sin^{-1}\left(\frac{f_{d,min}}{f_d}\right)}^{\sin^{-1}\left(\frac{f_{d,max}}{f_d}\right)} \cos(2\pi f_d\tau\sin\phi)d\phi\right. \\ & \left. -j\int_{\cos^{-1}\left(\frac{f_{d,min}}{f_d}\right)}^{\cos^{-1}\left(\frac{f_{d,max}}{f_d}\right)} \sin(2\pi f_d\tau\cos\phi)d\phi\right]. \end{aligned} \quad (43)$$

The sampled impulse response $h_{aj}[m]$ is obtained numerically by performing an inverse FFT on the frequency-sampled version of the amplitude of the frequency response.

Bi-Gaussian Doppler Spectrum

The bi-Gaussian power spectrum consists of two frequency-shifted Gaussian spectra. The COST 207 channel models [42], [27] specify two distinct bi-Gaussian Doppler spectra, GAUS1 and GAUS2, to be used in modeling long echos for urban and hilly terrain profiles. The normalized bi-Gaussian Doppler spectrum is given analytically by:

$$\begin{aligned} S_{bg}(f) &= A_{bg}\left[\frac{C_{g1}}{\sqrt{2\pi\sigma_{g1}^2}}\exp\left(-\frac{(f-f_{g1})^2}{2\sigma_{g1}^2}\right)\right. \\ & \left. +\frac{C_{g2}}{\sqrt{2\pi\sigma_{g2}^2}}\exp\left(-\frac{(f-f_{g2})^2}{2\sigma_{g2}^2}\right)\right] \end{aligned} \quad (44)$$

where σ_{g1} and σ_{g2} are standard deviations, f_{g1} and f_{g2} are center frequencies, C_{g1} and C_{g2} are power gains, and $A_{bg} = \frac{1}{C_{g1}+C_{g2}}$ is a normalization coefficient. If either $C_{g1} = 0$ or $C_{g2} = 0$, a frequency-shifted Gaussian Doppler spectrum is obtained. If both center frequencies are zero and the standard deviations are equal, a Gaussian Doppler spectrum results. The autocorrelation function can be obtained analytically as:

$$\begin{aligned} R_{bg}(\tau) &= A_{bg}C_{g1}\exp(-2\pi^2\sigma_{g1}^2\tau^2) \\ & +A_{bg}C_{g2}\exp(-2\pi^2\sigma_{g2}^2\tau^2). \end{aligned} \quad (45)$$

The sampled impulse response $h_{bj}[m]$ is obtained numerically by performing an inverse FFT on the frequency-sampled version of the amplitude of the frequency response.

Rounded Doppler Spectrum

A rounded PSD was proposed in [43] as an approximation to the measured PSD of the scatter component of fixed wireless channels at 2.5 GHz. It is cautioned however that the shape of the PSD is influenced by the center carrier frequency. The baseband normalized rounded Doppler spectrum is given by:

$$S_r(f) = C_r \left[a_0 + a_2 \left(\frac{f}{f_d} \right)^2 + a_4 \left(\frac{f}{f_d} \right)^4 \right] \quad |f| \leq f_d, \quad (46)$$

with:

$$C_r = \frac{1}{2 f_d \left[a_0 + \frac{a_2}{3} + \frac{a_4}{5} \right]} \quad (47)$$

being a normalization factor. It is seen that the rounded Doppler spectrum is actually a polynomial function of frequency, of order 4, where only the even powers are retained. The real numbers a_0, a_2, a_4 are the coefficients of the polynomial. For example, the fixed wireless channel model of IEEE 802.16 [43] uses the following parameters: $a_0 = 1$, $a_2 = -1.72$, $a_4 = 0.785$. Since the channel is modeled as Rician fading with a fixed LOS component, a Dirac delta is also present in the PSD at $f = 0$. The autocorrelation function can be obtained by taking the inverse Fourier transform of (46), and using Eqs. 2.531.2 and 2.633.2 of [31]:

$$\begin{aligned} R_r(\tau) &= 2C_r \left[a_0 \frac{\sin(2\pi f_d \tau)}{2\pi\tau} \right. \\ &+ \frac{a_2}{f_d^2} \sum_{k=0}^{2} k! \binom{2}{k} \frac{f_d^{2-k} \sin(2\pi f_d \tau + k\pi/2)}{(2\pi\tau)^{k+1}} \\ &\left. + \frac{a_4}{f_d^2} \sum_{k=0}^{4} k! \binom{4}{k} \frac{f_d^{4-k} \sin(2\pi f_d \tau + k\pi/2)}{(2\pi\tau)^{k+1}} \right] \quad (48) \end{aligned}$$

The sampled impulse response $h_r[m]$ is obtained numerically by performing an inverse FFT on the frequency-sampled version of the amplitude of the frequency response.

Doppler Filtering Equations

In order to reduce the effect of the Gibbs phenomenon attributable to truncation, the sampled impulse responses $\{h_D[m]\}$ for the Doppler filters above are multiplied by a window $\{w[m]\}$, e.g. a Hamming window $\{w_H[m]\}$, to obtain the windowed impulse response of the shaping filter:

$$h_w[m] = h_D[m] w_H[m], \quad (49)$$

for $m = 0, 1, \ldots, M-1$. The windowed impulse response is then normalized such that its total power is 1:

$$h_{norm}[m] = h_w[m] / \sqrt{\textstyle\sum_{m=0}^{M-1} |h_w[m]|^2}, \quad (50)$$

for $m = 0, 1, \ldots, M-1$. For brevity $\{h_{norm}[n]\}$ is denoted as $\{h[n]\}$ in the following.

The output of the Doppler filter in response to the input complex Gaussian noise process is:

$$\begin{aligned} y[n] &= \textstyle\sum_{m=0}^{M-1} h[m] x_G[n-m] \quad (51) \\ &= y_R[n] + j y_I[n] \quad (52) \end{aligned}$$

where $y_R[n] = \Re[y[n]]$ and $y_I[n] = \Im[y[n]]$, $n = 1, 2, 3, \ldots$. If the Doppler spectrum is symmetrical, then the Doppler filter impulse response is real, and:

$$\begin{aligned} y_R[n] &= \textstyle\sum_{m=0}^{M-1} h[m] x_{G,R}[n-m], \\ y_I[n] &= \textstyle\sum_{m=0}^{M-1} h[m] x_{G,I}[n-m]. \end{aligned}$$

If the Doppler spectrum is asymmetrical, then the Doppler filter impulse response $h[m] = h_R[m] + j h_I[m]$, $m = 0, 1, \ldots, M-1$, is in general complex, and:

$$y_R[n] = \textstyle\sum_{m=0}^{M-1} \left[h_R[m] x_{G,R}[n-m] - h_I[m] x_{G,I}[n-m] \right],$$

$$y_I[n] = \textstyle\sum_{m=0}^{M-1} \left[h_R[m] x_{G,I}[n-m] + h_I[m] x_{G,R}[n-m] \right].$$

C.3 Interpolation Filtering

The fading process must be sampled at a rate $f_s = 1/t_s$ equal to at least twice the cutoff frequency $f_{c,D}$ of the fading process. For the Jakes and flat Doppler spectra, the theoretical cutoff frequency is equal to the maximum Doppler shift, i.e. $f_{c,D} = f_d$. For the Gaussian Doppler spectrum, the cutoff frequency $f_{c,D}$ is related to the standard deviation of the Gaussian function, as detailed in Section III-C. Usually, a higher sampling rate is recommended, e.g. $f_s = 6$ to $12 f_{c,D}$ samples/s [14]. We choose a target sampling rate of $f_{s,t} = 10 f_{c,D}$.

The channel input sampling rate $R_s = 1/T_s$ is typically much larger than the target Doppler sampling rate $f_{s,t}$. Hence, samples of the generated fading process need to be interpolated by an expansion factor:

$$L = \lfloor R_s / f_{s,t} \rfloor. \quad (53)$$

The actual Doppler sampling rate is then:

$$f_s = \frac{R_s}{L} = \frac{R_s}{\lfloor R_s / f_{s,t} \rfloor}, \quad (54)$$

which is greater or equal to the target sampling rate.

To perform efficient interpolation, we use a combination of polyphase interpolation filtering and linear interpolation filtering [14]. To further reduce complexity, the polyphase interpolation factor L_P is kept below a chosen limit, with no constraint on the linear interpolation factor L_L. These interpolation factors are computed according to the following algorithm:

- If $L <= L_{P,max}$, only polyphase interpolation is used: $L_P = L$, $L_L = 1$.
- If $L > L_{P,max}$, a combination of polyphase and linear interpolation is used: $L_P = L_{P,min}$, $L_L = \text{round}(L/L_P)$, and the

overall interpolation factor is recomputed as $L = L_P L_L$. The Doppler sampling rate must also be recomputed as $f_s = R_s/L$. We choose $L_{P,max} = 20$ and $L_{P,min} = 10$. The polyphase and linear interpolation filtering operations are summarized below.

Polyphase Interpolation Filtering

The output of the polyphase interpolator is given by [44]:

$$z_P[n] = \sum_{i=-\infty}^{\infty} p_{((n))_{L_P}}[i] y\left[\lfloor n/L_P \rfloor - i\right] \quad (55)$$

where $\{p_l[i]\}$, $l = 0, 1, 2, \ldots, L_P - 1$ are a bank of L_P polyphase filters, derived from an interpolation filter $\{h_I[m]\}$ as:

$$p_{((n))_{L_P}}[i] = h_I[iL_P + ((n))_{L_P}] \quad (56)$$

where $((\cdot))_N$ denotes modulo N. From Eq. (55), the output samples $z_P[0]$, $z_P[L_P]$, $z_P[2L_P]$, ... are calculated using the polyphase filter $\{p_0[i]\}$. The output samples $z_P[1]$, $z_P[L_P + 1]$, $z_P[2L_P + 1]$, ... are calculated using the polyphase filter $\{p_1[i]\}$, and so forth. Hence, for each output sample only one of the L_P polyphase filters is used for interpolation. The length of each individual polyphase filter is $1/L_P$ times the length of the interpolation filter. Therefore, interpolation filtering using a polyphase structure requires only $1/L_P$ times the number of coefficient multiplications as would a direct structure, which results in a lower computational complexity.

The *ideal* interpolation filter should be an ideal lowpass filter with radian cutoff frequency π/L_P and gain L_P [44], i.e.:

$$h_{I,ideal}[m] = L_P \frac{\sin(\pi m/L_P)}{\pi m/L_P}, \ -\infty < m < \infty. \quad (57)$$

The *designed* interpolation filter $\{h_I[m]\}$ is a linear phase FIR filter which performs bandlimited interpolation using the nearest $2P$ non-zero samples (P being a chosen positive integer), and assumes that the input signal is bandlimited to αf_s, where α is chosen as 0.5 (recall that typically the chosen sampling rate f_s is several times greater than the fading process' cutoff frequency $f_{c,D}$; a smaller α can allow better stopband attenuation in the designed filter). It is designed using the `intfilt` function from the Signal Processing Toolbox, which returns a filter of length $2L_P P - 1$. The `intfilt` function makes uses of the `firls` function of the Signal Processing Toolbox, which designs a linear-phase FIR filter using least-squares error minimization. The filter returned by `intfilt` is extended by 1 to obtain the interpolation filter $\{h_I[m]\}$ of length $N_I = 2L_P P$. The L_P polyphase filters, each of length $N_p = N_I/L_P = 2P$, are then obtained through (56). We choose $P = 4$ in the software implementation.

Linear Interpolation Filtering

The impulse response of a linear interpolation filter with interpolation factor L_L is given by:

$$h_L[m] = 1 - |m|/L_L, \ |m| \leq L_L. \quad (58)$$

The output of the linear interpolator is then given by [14]:

$$z_L[n + m + 1] = z_L[n + m] + \frac{z_{P,up}[n + L_L] - z_L[n]}{L_L}, \quad (59)$$

for $m = 0, 1, \ldots, L_L - 2$, where the input sequence $\{z_{P,up}[n]\}$ is the upsampled (by a factor of L_L) output from the polyphase interpolator described above.

C.4 Path Gain Scaling

Let $\{z_k[n]\}$ denote the output sequence from the hybrid polyphase-linear interpolator for path k. The discrete-time complex path gains, $\{\tilde{a}_k[n] = \tilde{a}_k(nT_s)\}$, are obtained by scaling the sequence $\{z_k[n]\}$ to obtain the specified average path power gains, $\Omega_k = E[|\tilde{a}_k(t)|^2]$, $k = 1, 2, \ldots, K$:

$$\tilde{a}_k[n] = \sqrt{\Omega_k} z_k[n], \ \ k = 1, 2, \ldots, K. \quad (60)$$

If the channel is Rician fading with a K-factor of $K_{r,k}$ on path k, the path gains are obtained as:

$$\tilde{a}_k[n] = \sqrt{\Omega_k} \left[\frac{z_k[n]}{\sqrt{K_{r,k} + 1}} + \sqrt{\frac{K_{r,k}}{K_{r,k} + 1}} \right], \quad (61)$$

for $k = 1, 2, \ldots, K$. If the line-of-sight component on path k is subject to a phase shift of $f_{d,LOS,k}$ Hz, with an initial phase of $\theta_{LOS,k}$ radians, then the path gains are written as:

$$\tilde{a}_k[n] = \sqrt{\Omega_k} \left[\frac{z_k[n]}{\sqrt{K_{r,k} + 1}} + \sqrt{\frac{K_{r,k}}{K_{r,k} + 1}} e^{j(2\pi f_{d,LOS,k} + \theta_{LOS,k})} \right]. \quad (62)$$

IV. Multipath Fading Channel Objects and Application Programming Interface

This section briefly reviews the application programming interface (API) used in the Communications Toolbox' channel functions for constructing channel objects and specifying their properties. It also shows some examples on how to simulate the effect of a multipath fading channel on frames of input data, and then visualize the effects using a graphical user interface (GUI).

A. Rayleigh Channel Object with Identical Doppler Spectrum on Each Path

The code snippet below uses the `rayleighchan` function to create a Rayleigh channel object `h` with an input sample period `Ts`, a maximum Doppler shift `fd`, a vector of path delays `tau`, and a vector of average path power gains `pdb` (in dB). It then uses the `doppler.gaussian` function to create a Gaussian Doppler object `dop` with a standard deviation `sigmag`, and assigns it to the `DopplerSpectrum` property of the constructed channel object. All paths of the channel then have a Gaussian Doppler spectrum.

```
Ts = 1e-4;
fd = 100;
```

```
tau = [0 1e-5 3.5e-5 12e-5 15e-5 20e-5 50e-5];
pdb = [0 -1 -1 -3 -3 -4 -8];
h = rayleighchan(Ts, fd, tau, pdb);
sigmag = 1.2;
dop = doppler.gaussian(sigmag);
h.DopplerSpectrum = dop;
h

h =

           ChannelType: 'Rayleigh'
       InputSamplePeriod: 1.0000e-004
         DopplerSpectrum: [1x1 doppler.gaussian]
         MaxDopplerShift: 100
              PathDelays: [1x7 double]
           AvgPathGaindB: [0 -1 -1 -3 -3 -4 -8]
      NormalizePathGains: 1
            StoreHistory: 0
               PathGains: [1x7 double]
     ChannelFilterDelay: 4
    ResetBeforeFiltering: 1
     NumSamplesProcessed: 0
```

It is seen that the channel object `h` has a set of properties. The properties `InputSamplePeriod`, `MaxDopplerShift`, `PathDelays`, and `AvgPathGaindB` are set equal to `Ts`, `fd`, `tau`, and `pdb`, respectively. The property `NormalizePathGains`, which is set to 1, specifies that the sum of the average path gain powers should be 1. The property `ChannelFilterDelay` contains the value of N_1 (c.f. Section III-B): hence a delay of 4 is incurred in the simulation.

The following code snippet performs multipath channel filtering and channel visualization. It first sets the `StoreHistory` property of the channel object to 1: this is needed to store quantities used in the visualization. It then sets the `ResetBeforeFiltering` property to 0: this avoids resetting the state of the channel object between frames, hence preserving continuity of the fading process across frames. Indeed, the channel simulator uses a block approach: the `filter` function, which performs multipath channel filtering (it is an overloaded function, not to be confused with the `filter` function of the Signal Processing Toolbox), takes as inputs the channel object `h` and a block of `Nsamp` samples to be processed through the channel. It returns a complex output vector `y`. The `plot` function (it is also an overloaded function, not to be confused with the MATLAB® `plot` function) takes the channel object as argument, and opens up the channel visualization tool, which allows the user to visualize several quantities associated with the simulated object, such as impulse response, frequency response, phasor trajectory, and Doppler spectrum. This is repeated for `Nframes` frames.

```
h.StoreHistory = 1;
h.ResetBeforeFiltering = 0;
Nframes = 1000;
Nsamp = 1000;
for i = 1:Nframes
    input = ones(1,Nsamp);
    y = filter(h, input);
    plot(h);
end
h

h =

           ChannelType: 'Rayleigh'
       InputSamplePeriod: 1.0000e-004
         DopplerSpectrum: [1x1 doppler.gaussian]
         MaxDopplerShift: 100
              PathDelays: [1x7 double]
           AvgPathGaindB: [0 -1 -1 -3 -3 -4 -8]
      NormalizePathGains: 1
            StoreHistory: 1
               PathGains: [1000x7 double]
     ChannelFilterDelay: 4
    ResetBeforeFiltering: 0
     NumSamplesProcessed: 1000000
```

The property `PathGains` is a matrix containing the values of $\{\tilde{a}_k[n] = \tilde{a}_k(nT_s)\}$, $k = 1, 2, \ldots, K$ for the last frame: the k^{th} column contains the values corresponding to the k^{th} path. The property `NumSamplesProcessed` keeps track of the number of input samples processed so far, which is `Nframes` * `Nsamp` = 1e6.

Fig. 3 is a snapshot of the channel visualization tool, illustrating the channel impulse response, whose amplitudes are time-varying because of the fading. The vertical lines correspond to the delays of the actual channel impulse response, as specified in `PathDelays`. The solid points along the solid curve (which is the smoothed bandlimited impulse response) correspond to the delays of the transformed, symbol-spaced channel impulse response: it is seen that there are 14 delays in the bandlimited symbol-spaced channel impulse response, as compared to 7 in the non-symbol-spaced one.

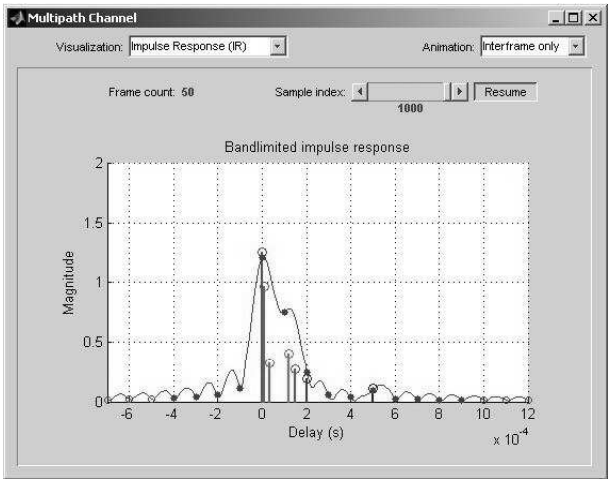

Fig. 3. Snapshot of the bandlimited impulse response for a Rayleigh channel.

B. Rician Channel Object with Different Doppler Spectra on Each Path

The example below creates a Rician channel object, and assigns a different K-factor and a different Doppler spectrum to each one of its path. The code snippet given above can then be used to filter blocks of data through the channel, and visualize quantities using the channel visualization tool. Fig. 4 is a snapshot of the scattering function of the channel, i.e. a 3-dimensional plot of the Doppler spectrum versus multipath delay.

```
Ts = 1e-4;
fd = 100;
kFactor = [3 1 0.2 0];
tau = [0 1e-5 1.5e-5 3e-5];
pdb = [0 -1 -2 -2.5];
h = ricianchan(Ts, fd, kFactor, tau, pdb);
h.DopplerSpectrum = [doppler.jakes
                     doppler.ajakes([-1 0.8])
                     doppler.rjakes([0 0.6])
                     doppler.rounded];
```

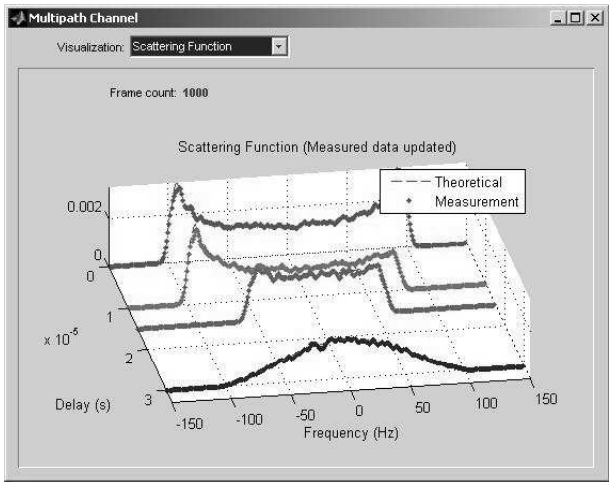

Fig. 4. Snapshot of the scattering function for a Rician channel.

V. Numerical Results

In this section, we evaluate the performance of the channel simulator in terms of the probability density function (pdf) of the real fading envelope $\{r[n] = |\tilde{a}[n]|\}$, and the autocovariance and power spectrum of the complex fading process $\{\tilde{a}[n]\}$. We only look at the statistics of the first path, since all paths have the same Doppler spectrum. The autocovariance is calculated using the `xcov` function, and the power spectrum using the `spectrum.welch` and `psd` functions (with a Hamming window specified), from the Signal Processing Toolbox.

Figs. 5, 6 and 7 show these quantities for the example of Section IV, where the Doppler spectrum is Gaussian. Only the real part of the autocovariance is plotted, as the imaginary part from the simulation is close to 0 (it should theoretically be zero). There is a close fit for all quantities, within the ranges of practical interest.

Figs. 8 and 9 show the autocovariance (real part) and power spectrum for a Rayleigh fading channel with a Jakes Doppler spectrum, and $f_d = 100$ Hz. The theoretical spectrum goes to infinity at $f = f_d$ and $-f_d$, hence only a finite approximation can be given by the simulator. The autocovariance shows some discrepancy at higher lags, but this is due to the small number of coefficients used for the Doppler impulse response: this speed/accuracy tradeoff allows a faster simulation.

Figs. 10 and 11 show the autocovariance (real part) and power spectrum for a Rayleigh fading channel with a flat Doppler spectrum, and $f_d = 100$ Hz. There is a close fit for all quantities, within the ranges of practical interest.

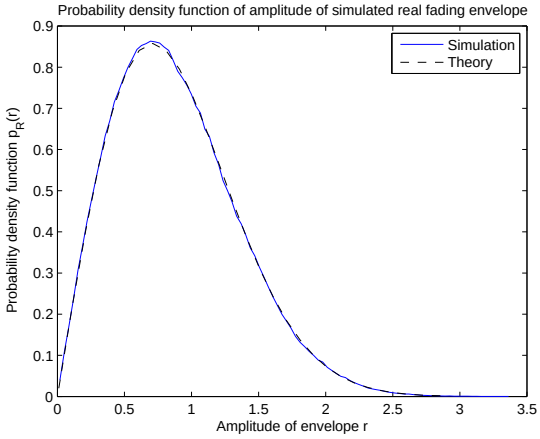

Fig. 5. Probability density function of the real fading envelope for a Rayleigh channel with a Gaussian Doppler spectrum with variance $\sigma_g = 1.2$.

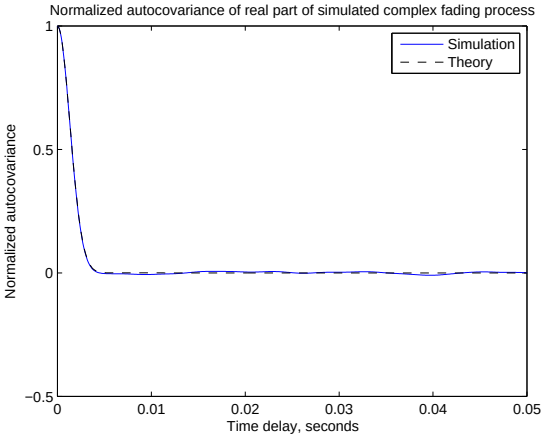

Fig. 6. Autocovariance (real part) of the complex fading process for a Rayleigh channel with a Gaussian Doppler spectrum with variance $\sigma_g = 1.2$.

Figs. 12 and 13 illustrate the autocovariance (real part) and power spectrum for a Rayleigh fading channel with a rounded Doppler spectrum, and $f_d = 100$ Hz. The coefficients of the spectrum are those used by the IEEE 802.16 channel model.

Figs. 14 and 15 show the autocovariance (real part) and power spectrum for a Rayleigh fading channel with a restricted Jakes Doppler spectrum, with $f_{d,min} = 20$ Hz and $f_{d,max} = 80$ Hz, and a support Doppler frequency of $f_d = 100$ Hz.

Figs. 16 and 17 show the real and imaginary parts of the autocovariance for a Rayleigh fading channel with an asymmetrical Jakes Doppler spectrum, with $f_{d,min} = -100$ Hz and $f_{d,max} = 0$ Hz, and a support Doppler frequency of $f_d = 100$ Hz. Fig. 18 gives the corresponding power spectrum.

Figs. 19 and 20 show the real and imaginary parts of the autocovariance for a Rayleigh fading channel with a bi-Gaussian Doppler spectrum, while Fig. 21 gives the corresponding power spectrum. The parameters are chosen as those of the COST 207 GAUS1 Doppler model: $\sigma_{g1} = 0.05 * f_d$, $\sigma_{g2} = 0.1 * f_d$, $f_{g1} = -0.8 * f_d$, $f_{g2} = 0.4 * f_d$, $C_{g1}/C_{g2} = 10$, where the Doppler frequency is chosen here as $f_d = 100$.

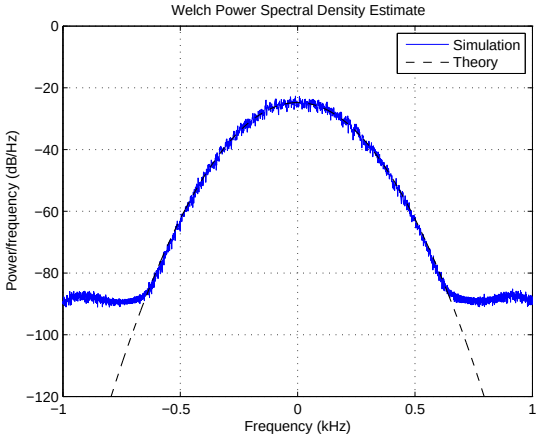

Fig. 7. Power spectrum of the complex fading process for a Rayleigh channel with a Gaussian Doppler spectrum with variance $\sigma_g = 1.2$.

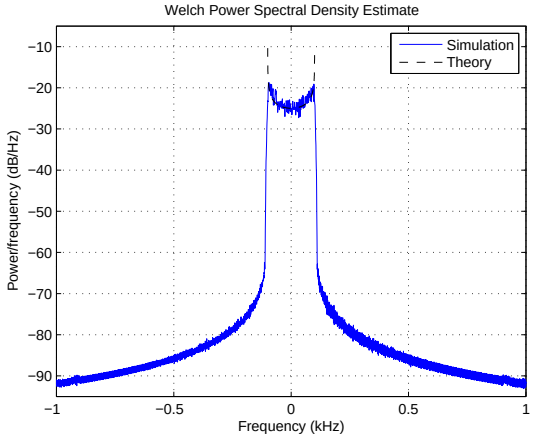

Fig. 9. Power spectrum of the complex fading process for a Rayleigh channel with a Jakes Doppler spectrum.

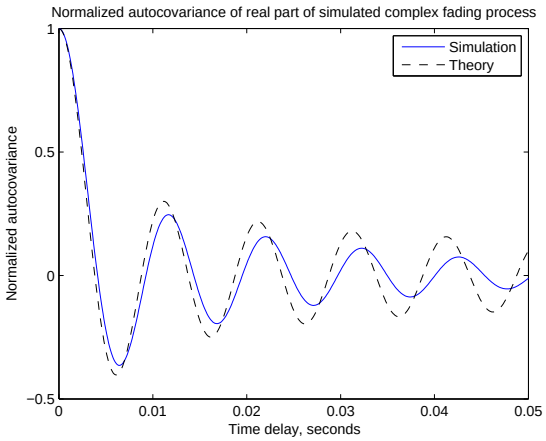

Fig. 8. Autocovariance (real part) of the complex fading process for a Rayleigh channel with a Jakes Doppler spectrum.

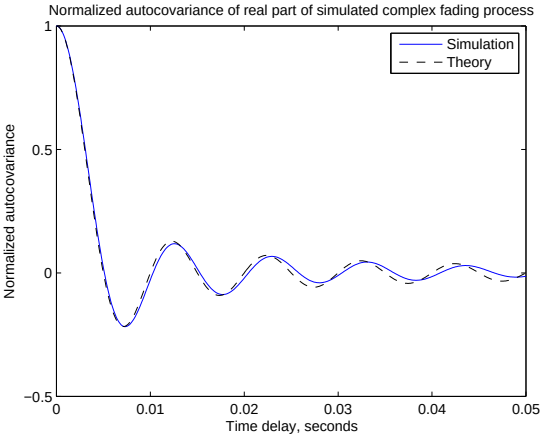

Fig. 10. Autocovariance (real part) of the complex fading process for a Rayleigh channel with a flat Doppler spectrum.

VI. Additional Resources

The function `stdchan` from the Communications Toolbox allows one to construct a channel object from a set of standardized channel models. The currently available channel models are: COST 207 [27], GSM/EDGE [45], [46], 3GPP TR.25.943 [47], ITU-R 3G [48], and ITU-R HF [37]. The demos "COST 207 and GSM/EDGE Channel Models" and "HF Ionospheric Channel Models" in the Communications Toolbox illustrate some of these channel models.

VII. Conclusion

This paper presented an object-oriented software implementation of a multipath fading channel, using the MATLAB® language. The algorithm is based on a combination of Doppler filtering, polyphase and linear interpolation filtering to simulate the Doppler spreading, and on a bandlimited representation of the channel to simulate the time spreading using symbol-spaced channel filtering. Numerical results show a good match with theoretical results for the pdf, autocovariance and power spectrum, for seven different commonly used Doppler spectra.

References

[1] R. H. Clarke, "A statistical theory of mobile-radio reception," *Bell Sys. Tech. J.*, vol. 47, no. 6, pp. 957–1000, July-Aug. 1968.

[2] A. Papoulis, *Probability, Random Variables, and Stochastic Processes*, McGraw-Hill, 1st edition, 1965.

[3] M. Nakagami, "The *m*-distribution–a general formula of intensity distribution of rapid fading," in *Statistical Methods in Radio Wave Propagation*, W. C. Hoffman, Ed., pp. 3–36. Pergamon, Elmsford, NY, 1960.

[4] M. J. Gans, "A power-spectral theory of propagation in the mobile-radio environment," *IEEE Trans. Veh. Technol.*, vol. VT-21, no. 1, pp. 27–38, Feb. 1972.

[5] W. C. Jakes, *Microwave Mobile Communications*, Wiley, 1974.

[6] P. A. Bello, "Characterization of randomly time-variant linear channels," *IEEE Trans. Commun. Syst.*, vol. CS-11, no. 4, pp. 360–393, Dec. 1963.

[7] P. Dent, G. Bottomley, and T. Croft, "Jakes fading model revisited," *IEE Electronics Letters*, vol. 29, no. 3, pp. 1162–1163, June 24th 1993.

[8] Y. Li and X. Huang, "The simulation of independent Rayleigh faders," *IEEE Trans. Commun.*, vol. 50, no. 9, pp. 1503–1514, Sept. 2002.

[9] S. O. Rice, "Mathematical analysis of random noise," *Bell Sys. Tech. J.*, vol. 23, pp. 282–332, July 1944.

[10] S. O. Rice, "Mathematical analysis of random noise," *Bell Sys. Tech. J.*, vol. 24, pp. 46–156, Jan. 1945.

[11] M. Patzold, *Mobile Fading Channels*, Wiley, 2002.

[12] M. Patzold, "On the stationarity and ergodicity of fading channel simu-

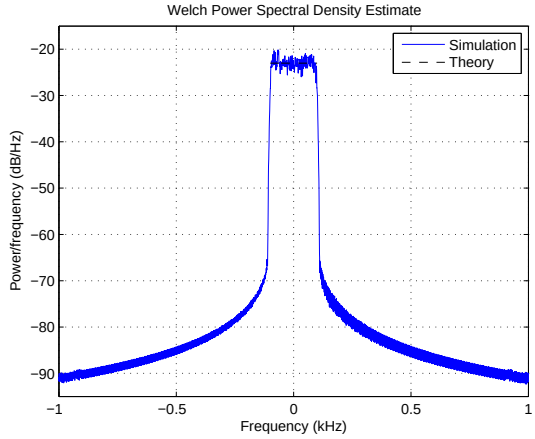

Fig. 11. Power spectrum of the complex fading process for a Rayleigh channel with a flat Doppler spectrum.

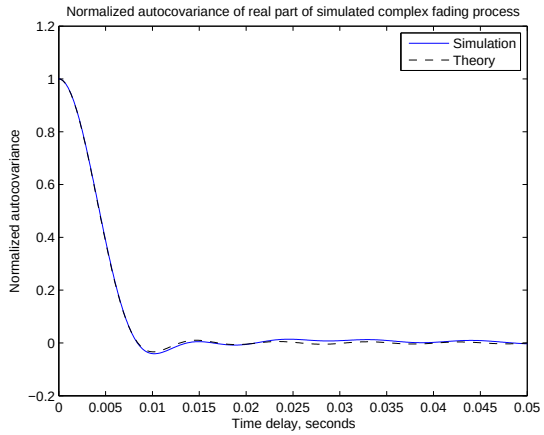

Fig. 12. Autocovariance (real part) of the complex fading process for a Rayleigh channel with a rounded Doppler spectrum.

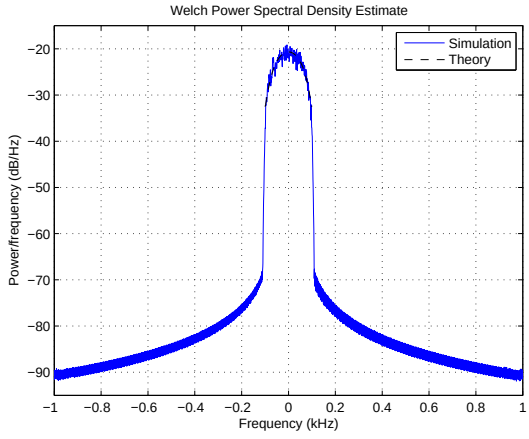

Fig. 13. Power spectrum of the complex fading process for a Rayleigh channel with a rounded Doppler spectrum.

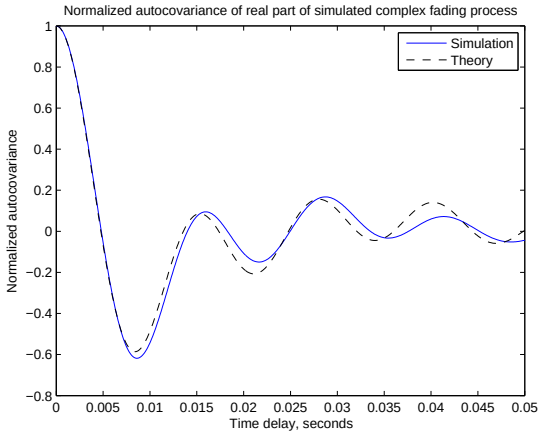

Fig. 14. Autocovariance (real part) of the complex fading process for a Rayleigh channel with a restricted Jakes Doppler spectrum, with $f_{d,min} = 20$ Hz and $f_{d,max} = 80$ Hz.

lators basing on Rice's sum-of-sinusoids," in *Proc. IEEE PIMRC*, 2003, pp. 1521–1523.

[13] D. Verdin and T. Tozer, "Generating a fading process for the simulation of land-mobile radio communications," *IEE Electronics Letters*, vol. 29, no. 23, pp. 2011–2012, Nov. 11th 1993.

[14] M. C. Jeruchim, P. Balaban, and K. S. Shanmugan, *Simulation of Communication Systems - Modeling, Methodology, and Techniques*, Kluwer Academic/Plenum Publishers, 2nd edition, 2000.

[15] P. Castoldi, R. Raheli, and G. Marino, "An efficient time-discrete symbol-spaced simulation model of mobile radio channels," in *Proc. IEEE PIMRC*, 1994, pp. 1300–1304.

[16] A. Anastasopoulos and K. M. Chugg, "An efficient method for simulation of frequency-selective isotropic Rayleigh fading," in *Proc. IEEE VTC*, 1997, pp. 2084–2088.

[17] D. Schafhuber, G. Matz, and F. Hlawatsch, "Simulation of wideband mobile radio channels using subsampled ARMA models and multistage interpolation," in *IEEE Workshop on Statistical Signal Processing*, 2001, pp. 571–574.

[18] C. Komninakis and J. F. Kirshman, "Fast Rayleigh fading simulation with an IIR filter and polyphase interpolation," *RF Design*, pp. 24–34, July 2004.

[19] K. E. Baddour and N. C. Beaulieu, "Autoregressive modeling for fading channel simulation," *IEEE Trans. Wireless Commun.*, vol. 4, no. 4, pp. 1650–1662, July 2005.

[20] J. I. Smith, "A computer generated multipath fading simulation for mobile radio," *IEEE Trans. Veh. Technol.*, vol. VT-24, no. 3, pp. 39–40, Aug. 1975.

[21] T. S. Rappaport, *Wireless Communications - Principles and Practice*, Prentice Hall PTR, 1st edition, 1996.

[22] D. J. Young and N. C. Beaulieu, "The generation of correlated Rayleigh random variates by Inverse Discrete Fourier Transform," *IEEE Trans. Commun.*, vol. 48, no. 7, pp. 1114–1127, July 2000.

[23] S. A. Fechtel, "A novel approach to modeling and efficient simulation of frequency-selective fading radio channels," *IEEE J. Select. Areas Commun.*, vol. 11, no. 3, pp. 422–430, 1993.

[24] P. Hoeher, "A statistical discrete-time model for the WSSUS multipath channel," *IEEE Trans. Veh. Technol.*, vol. 41, no. 4, pp. 461–468, Nov. 1992.

[25] G. L. Turin *et al.*, "A statistical model of urban multipath propagation," *IEEE Trans. Veh. Technol.*, vol. VT-21, no. 1, pp. 1–9, Feb. 1972.

[26] J. G. Proakis, *Digital Communications*, McGraw-Hill, 4th edition, 2001.

[27] COST 207, "Digital land mobile radio communications," Office for Official Publications of the European Communities, Final report, Luxembourg, 1989.

[28] G. Marsaglia and W. W. Tsang, "The Ziggurat method for generating random variables," *Journal of Statistical Software*, vol. 5, no. 8, 2000.

[29] W. C. Lee, *Mobile Communications Engineering: Theory and Applications*, McGraw-Hill, 1998.

[30] E. N. Gilbert, "Energy reception for mobile radio," *Bell Sys. Tech. J.*, vol. 44, no. 8, pp. 1779–1803, Oct. 1965.

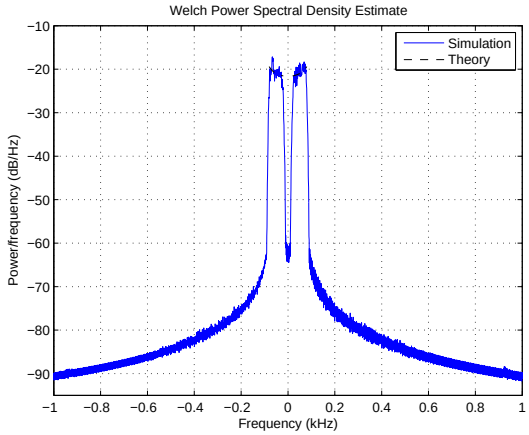

Fig. 15. Power spectrum of the complex fading process for a Rayleigh channel with a restricted Jakes Doppler spectrum, with $f_{d,min} = 20$ Hz and $f_{d,max} = 80$ Hz.

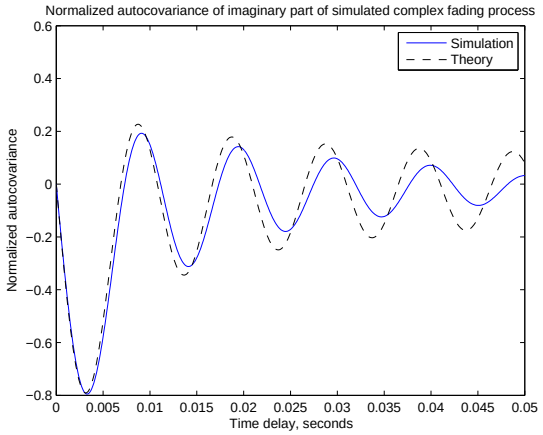

Fig. 17. Autocovariance (imaginary part) of the complex fading process for a Rayleigh channel with an assymetrical Jakes Doppler spectrum, with $f_{d,min} = -100$ Hz and $f_{d,max} = 0$ Hz.

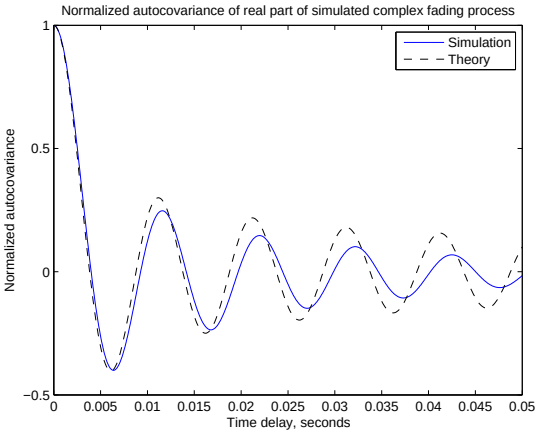

Fig. 16. Autocovariance (real part) of the complex fading process for a Rayleigh channel with an assymetrical Jakes Doppler spectrum, with $f_{d,min} = -100$ Hz and $f_{d,max} = 0$ Hz.

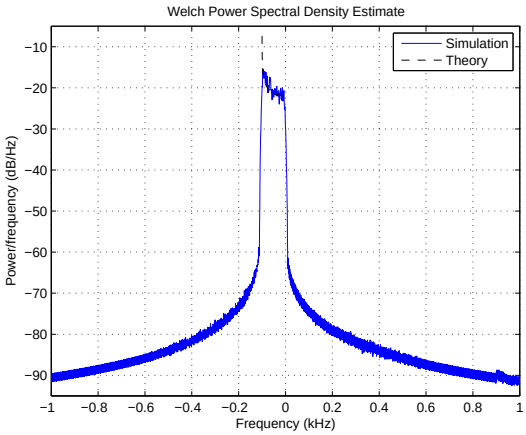

Fig. 18. Power spectrum of the complex fading process for a Rayleigh channel with an assymetrical Jakes Doppler spectrum, with $f_{d,min} = -100$ Hz and $f_{d,max} = 0$ Hz.

[31] I. S. Gradshteyn and I. M. Ryzhik, *Table of Integrals, Series, and Products*, Academic Press, 6th edition, 2000.

[32] R. H. Clarke and W. L. Khoo, "3-D mobile radio channel statistics," *IEEE Trans. Veh. Technol.*, vol. 46, no. 3, pp. 798–799, Aug. 1997.

[33] ANSI J-STD-008, "Personal station-base station compatibility requirements for 1.8 to 2.0 GHz Code Division Multiple Access (CDMA) Personal Communications Systems," Mar. 1995.

[34] D. C. Cox, "Delay Doppler characteristics of multipath propagation at 910 MHz in a suburban mobile radio environment," *IEEE Trans. on Antennas and Propagation*, vol. AP-20, no. 5, pp. 625–635, Sept. 1972.

[35] C. C. Watterson, J. R. Juroshek, and W. D. Bensema, "Experimental confi rmation of an HF channel model," *IEEE Trans. Commun. Technol.*, vol. COM-18, no. 6, pp. 792–803, Dec. 1970.

[36] L. Ehrman, L. B. Bates, J. F. Eschle, and J. M. Kates, "Real-time software simulation of the HF radio channel," *IEEE Trans. Commun.*, vol. COM-30, no. 8, pp. 1809–1817, Aug. 1982.

[37] Recommendation ITU-R F.1487, "Testing of HF modems with bandwidths of up to about 12 kHz using ionospheric channel simulators," 2000.

[38] P. A. Bello, "Aeronautical channel characterizations," *IEEE Trans. Commun.*, vol. 21, no. 21, pp. 548–563, May 1973.

[39] K. Hofbauer and G. Kubin, "Aeronautical voice radio channel modelling and simulation - A tutorial review," in *Proc. of the 2nd International Conference on Research in Air Transportation (ICRAT 2006), Belgrade, Serbia*, July 2006.

[40] E. Haas, "Aeronautical channel modeling," *IEEE Trans. Veh. Technol.*, vol. 51, no. 2, pp. 254–264, Mar. 2002.

[41] P. Hoeher and E. Haas, "Aeronautical channel modeling at VHF-band," in *Proc. IEEE VTC*, July 1999, pp. 1961–1966.

[42] COST 207 WG1, "Proposal on channel transfer functions to be used in GSM tests late 1986," COST 207 TD (86) 51 Rev. 3, Sept. 1986.

[43] IEEE 802.16 Broadband Wireless Access Working Group, "Channel models for fi xed wireless applications," IEEE 802.16a-03/01, 2003-06-27.

[44] R. E. Crochiere and L. R. Rabiner, "Interpolation and decimation of digital signals - A tutorial review," *Proc. IEEE*, vol. 69, no. 3, pp. 300–331, Mar. 1981.

[45] 3GPP, "Technical specifi cation group GSM/EDGE radio access network; radio transmission and reception (Release 7)," TS 45.005 V7.9.0 (2007-02), Feb. 2007.

[46] 3GPP, "Technical specifi cation group gsm/edge radio access network; radio transmission and reception (release 1999)," TS 05.05 V8.20.0 (2005-11), Nov. 2005.

[47] 3GPP, "Technical specifi cation group radio access networks; deployment aspects," TR 25.943 V6.0.0 (2004-12), Dec. 2004.

[48] Recommendation ITU-R M.1225, "Guidelines for evaluation of radio transmission technologies for IMT-2000," 1997.

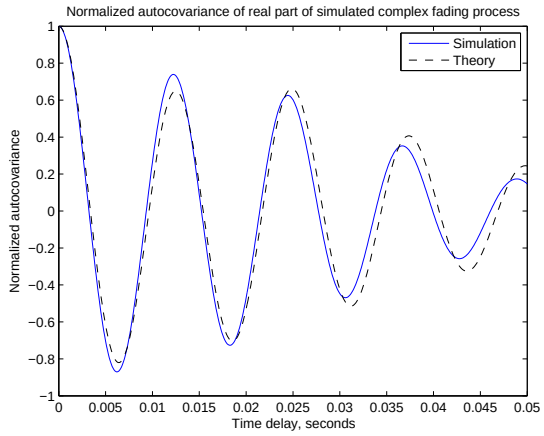

Fig. 19. Autocovariance (real part) of the complex fading process for a Rayleigh channel with a bi-Gaussian Doppler spectrum, with parameters corresponding to the COST 207 GAUS1 Doppler model.

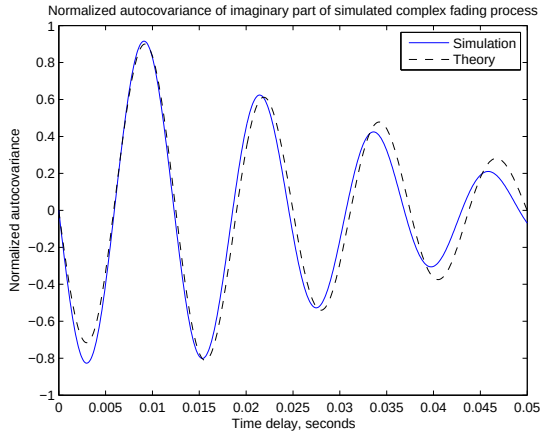

Fig. 20. Autocovariance (imaginary part) of the complex fading process for a Rayleigh channel with a bi-Gaussian Doppler spectrum, with parameters corresponding to the COST 207 GAUS1 Doppler model.

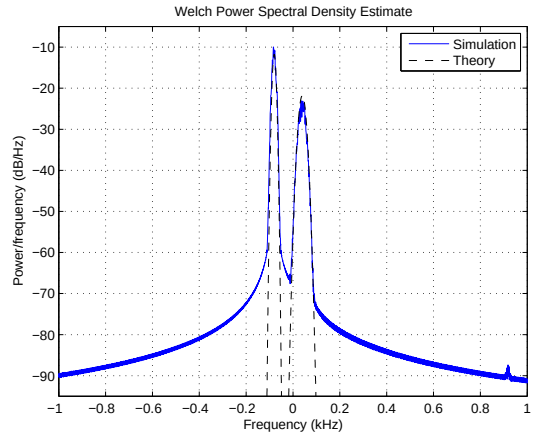

Fig. 21. Power spectrum of the complex fading process for a Rayleigh channel with a bi-Gaussian Doppler spectrum, with parameters corresponding to the COST 207 GAUS1 Doppler model.